

Revision 1

Karlditmarite, $\text{Cu}_9\text{O}_4(\text{PO}_4)_2(\text{SO}_4)_2$, the first copper phosphate-sulfate mineral from the Tolbachik volcano

Word count 6502

Oleg I. Siidra^{1,2*}, Evgeni V. Nazarchuk¹, Leonid A. Pautov³, Artem S. Borisov⁴, Anatoly N. Zaitsev⁵, Evgeniya Yu. Avdontseva¹

¹Department of Crystallography, St. Petersburg State University, University Embankment 7/9,
199034 St. Petersburg, Russia

²Kola Science Center, Russian Academy of Sciences, Apatity 184200, Murmansk Region,
Russia

³Fersman Mineralogical Museum, Russian Academy of Sciences, Leninskiy pr. 18-2, 119071
Moscow, Russia

⁴Institut für Geowissenschaften der Universität Kiel, Olshausenstr. 40, D-24098 Kiel, Germany

⁵Department of Mineralogy, St. Petersburg State University, University Embankment 7/9,
199034 St. Petersburg, Russia

*E-mail: o.siidra@spbu.ru

Abstract

Karlditmarite (IMA 2021-003), $\text{Cu}_9\text{O}_4(\text{PO}_4)_2(\text{SO}_4)_2$, is a new mineral species from an active Arsenatnaya fumarole, Tolbachik volcano, Kamchatka peninsula. Karlditmarite occurs as green prismatic crystals. The mineral is biaxial (-), with $\alpha = 1.872(2)$, $\beta = 1.835(3)$, and $\gamma =$

1.810(3) (589 nm). Under the microscope, karlditmarite is green with weak pleochroism. Electron microprobe analysis provided the empirical formula $(\text{Cu}_{8.614}\text{Zn}_{0.175}\text{Al}_{0.053}\text{Ca}_{0.019}\text{Fe}_{0.157})(\text{P}_{1.574}\text{S}_{1.814}\text{As}_{0.444}\text{V}_{0.109}\text{Si}_{0.059})\text{O}_{20}$. Karlditmarite is triclinic, $P\bar{1}$: $a = 6.1256(7)$ Å, $b = 7.9192(8)$ Å, $c = 7.9866(8)$ Å, $\alpha = 75.173(2)^\circ$, $\beta = 86.639(2)^\circ$, $\gamma = 88.660(2)^\circ$, $V = 373.87(7)$. The crystal structure ($R_1 = 0.039$) is unique. The ${}^2_{\infty}[\text{Cu}_9\text{O}_4]^{10+}$ layer in karlditmarite can be described as composed of six-membered rings, in which two of the six OCu_4 tetrahedra share a common edge. The interlayer space between the bends of the highly corrugated ${}^2_{\infty}[\text{Cu}_9\text{O}_4]^{10+}$ layers hosts phosphate tetrahedra, whereas sulfate tetrahedra are placed above the centers of the rings. Karlditmarite is the first anhydrous Cu phosphate-sulfate mineral among more than one hundred copper oxysalt mineral species known from the active fumaroles.

Phosphorus geochemistry in fumarolic environments is discussed.

Keywords: karlditmarite; phosphates; sulfates; copper; oxocentered complexes; fumaroles; Tolbachik volcano

1. Introduction

Tolbachik volcano (Kamchatka) is the well-known locality due to recent basaltic eruptions (1975-1976, 2012-2013: [Fedotov 1984](#); [Belousov et al. 2015](#)), and strong fumarolic activity ([Menyailov and Nikitina 1980](#); [Zelenski et al. 2014](#)). Escaping hot, up to 1070 °C, H₂O-rich, H₂S, HF, HCl, CO₂ and SO₂-bearing gases, containing up to 880 ppm of trace elements, in combination with high oxygen fugacity led to a remarkable mineralogy of fumarolic deposits (e.g. [Chaplygin et al. 2016](#), [Pekov et al. 2020](#), [Borisov et al. 2024](#)). More than 500 minerals are known from fumarolic deposits and > 130 mineral species were discovered for the first time at Tolbachik. Most of fumarolic minerals are represented by oxysalt and halide minerals. Copper oxide and oxysalt

mineralization is exceptional at Tolbachik fumaroles and includes diverse sulfates, arsenates, vanadates and selenites, but surprisingly, no copper phosphate minerals were described from fumarolic deposits until recently.

Phosphorus as minor and even major component is present in several fumarolic minerals, including forsterite (up to 12.9 wt% P₂O₅, [Shchipalkina et al. 2019](#)), sanidine and filatovite (up to 5.0 wt%, [Shchipalkina et al. 2020a](#)), fluorophlogopite (up to 0.9 wt%, [Shchipalkina et al. 2020b](#)), leucite (up to 0.9 wt%, [Shchipalkina et al. 2020c](#)). Copper phosphate minerals (with dominant (PO₄)³⁻ group) in fumaroles were first described in 2021 by [Siidra et al. \(2021a,b, 2022\)](#): they are paulgrothite Cu₉Fe³⁺O₄(PO₄)₄Cl, milkovoite Cu₄O(PO₄)(AsO₄) and antipovite Cu₅O₂(PO₄)₂. Following mineralogical studies of fumarolic mineralization at Tolbachik revealed more phosphate (wagnerite, chladniite, fluorapatite) and P-bearing (pliniusite, arsenowagnerite, rhabdoborite group) minerals. However, phosphates are less common minerals in oxidizing fumarolic environments compared with e.g. sulfates or arsenates, and their appearance is restricted to small-size outcrops.

In this contribution we describe karlditmarite (IMA 2021-003), Cu₉O₄(PO₄)₂(SO₄)₂, approved by the Commission on New Minerals, Nomenclature and Classification of the International Mineralogical Association (IMA-CNMNC). The holotype specimen is deposited in the collections of the Fersman Mineralogical Museum, Moscow, Russia, catalogue number 5589/1. Karlditmarite is the first Cu phosphate-sulfate mineral among more than one hundred various copper oxysalts known from the active fumaroles. We also briefly discuss the phosphorus geochemistry in fumarolic environments.

2. Materials and methods

2.1 Mineral name and occurrence

Karlditmarite is named in honor of a Baltic German geologist and explorer Karl Bernhard Woldemar Ferdinand von Ditmar (August 27, 1822 – April 13, 1892) born in Fennern (Vändra),

Estonia. Karl von Ditmar pursued his education in geology and mineralogy at the University of Dorpat (currently the University of Tartu) from 1841 to 1846. He spent two years at the Freiberg Mining Academy, and the Universities of Leipzig and Berlin after defending his dissertation in 1847. Karl von Ditmar initiated scientific communication with the St. Petersburg Academy of Sciences in late 1848. This partnership outlined von Ditmar's primary research focus, which was Kamchatka exploration. During his expeditions from 1851 to 1855, he acquired material for geological studies (Ditmar, 1860). Ditmar's seminal work "Reisen und Aufenthalt in Kamtschatka in den Jahren 1851–1855" (Travels and stay in Kamchatka in the years 1851–1855) (Figure 1a,b) contains a substantial portion of his observations (Ditmar, 1890). In addition to descriptive research, von Ditmar collaborated with the Russian Geographical Society to map Kamchatka. This resulted in the first geological maps of the Kamchatka Peninsula (Ditmar, 1856) (Figure 1c,d), which were published in the Proceedings of the Imperial Academy of Sciences with geological and petrographic notes.

Karlditmarite is a product of fumarolic activity. It was found in the Arsenatnaya fumarole, at the Second Scoria Cone of the Northern Breakthrough of the Great Fissure Tolbachik Eruption in Kamchatka, Russia. The Second Scoria Cone is located approximately 18 km SSW of the active shield volcano Ploskiy Tolbachik (Fedotov and Markhinin, 1983). Karlditmarite is deposited directly from volcanic gas emissions as a sublimate. The temperature of gases at the sampling location in September, 2017 was approximately 350 °C. All the recovered samples were packed and isolated when collected to avoid any contact with the external atmosphere. Associated minerals (Figure 2) are langbeinite, euchlorine, anhydrite, itelmenite, tenorite and paulgrothite $\text{Cu}_9\text{Fe}^{3+}\text{O}_4(\text{PO}_4)_4\text{Cl}$, milkovoite $\text{Cu}_4\text{O}(\text{PO}_4)(\text{AsO}_4)$ and antipovite $\text{Cu}_5\text{O}_2(\text{PO}_4)_2$.

2.2 Physical and optical properties

Karlditmarite's prismatic crystals (Figure 2) are olive-green and reach up 50 μm but usually measure from 1 to 10 μm in size. They are transparent to translucent with a vitreous luster, have a

light-green streak. Karlditmarite is brittle with no cleavage and parting observed. The hardness was not measured because of the small size of the crystals. The density could not be measured because of the paucity of available material. The calculated density is $4.606 \text{ g}\cdot\text{cm}^{-3}$ based on the empirical formula. Karlditmarite is insoluble in H_2O .

Optically, karlditmarite is biaxial (–), with $\alpha = 1.872(2)$, $\beta = 1.835(3)$, and $\gamma = 1.810(3)$ (589 nm). The calculated $2V$ value is 99.7° . Under the microscope, karlditmarite is green with weak pleochroism. The Gladstone-Dale compatibility (Mandarino, 2007) is $1 - (K_p/K_c) = -0.0376$ (excellent).

2.3 Chemical composition

Chemical analyses (N = 10) (Table 1) were performed using Si(Li) – energy-dispersive spectrometer (EDS) with ultrathin ATW-2 window and INCA Energy 350 (Oxford Instruments) at the accelerating voltage of 15 kV and probe current 0.5 nA, 5-15 μm beam diameter at the Fersman Mineralogical Museum. The analytical conditions used were 15 kV accelerating voltage, 0.5 nA beam current and a beam diameter of 5-15 μm .

The empirical formula calculated on the basis of 20 oxygen *pfu* is $(\text{Cu}_{8.614}\text{Zn}_{0.175}\text{Al}_{0.053}\text{Ca}_{0.019}\text{Fe}_{0.157})(\text{P}_{1.574}\text{S}_{1.814}\text{As}_{0.444}\text{V}_{0.109}\text{Si}_{0.059})\text{O}_{20}$. The simplified formula is $(\text{Cu,Zn,Fe,Al,Ca})_9\text{O}_4[(\text{P,As})\text{O}_4]_2[(\text{S,V,Si})\text{O}_4]_2$. The ideal formula is $\text{Cu}_9\text{O}_4(\text{PO}_4)_2(\text{SO}_4)_2$, which requires CuO 70.33, P_2O_5 13.94, SO_3 15.73, total 100 wt. %.

Crystal structure considerations show that mineral is anhydrous and does not contain CO_3 groups.

2.4 Powder X-ray diffraction

X-ray powder diffraction data were obtained using a Rigaku R-Axis Rapid II curved imaging plate diffractometer with $\text{CoK}\alpha$ radiation. A Gandolfi-like motion on the ϕ and ω axes was used to randomize diffraction from the sample. Observed d-values and intensities were derived. Data (in \AA for $\text{CoK}\alpha$) are given in Table S1. Unit-cell parameters refined from the powder

data in $P\bar{1}$ space group are: $a = 6.114(8) \text{ \AA}$, $b = 7.931(1) \text{ \AA}$, $c = 7.989(9) \text{ \AA}$, $\alpha = 75.06(1)^\circ$, $\beta = 86.55(9)^\circ$, $\gamma = 88.48(1)^\circ$, $V = 373.6(6) \text{ \AA}^3$.

2.5 Single-crystal X-ray diffraction

Single crystal of karlditmarite selected for X-ray diffraction analysis was glued onto glass filament and arranged in a Bruker Apex II Duo diffractometer operating with $\text{MoK}\alpha$ radiation at 50 kV and 0.6 mA. More than a hemisphere of data was collected with a frame width of 0.5° in ω , and 250 s spent counting for each frame. The data were integrated and corrected for absorption applying a multiscan type model using the Rigaku Oxford Diffraction programs CrysAlis Pro. The unit-cell parameters were calculated by the least-squares method. The structure was solved by direct methods and refined using SHELXT software (Sheldrick, 2015). The parameters of the X-ray diffraction experiment and structure refinement are given in Table 2. Table 3 contains the coordinates, bond-valence sums and equivalent isotropic displacement parameters of atoms. Selected interatomic distances are given in Table 4. Bond valences were calculated using parameters from Gagné and Hawthorne (2015).

3. Crystal structure

The crystal structure of karlditmarite contains six symmetrically independent Cu sites (Figure 3, Table 4) with three types of coordination environments taking into account all Cu-O bond lengths $< 2.85 \text{ \AA}$. Cu1, Cu3 and Cu4 have similar distorted square pyramidal $[(40)+0]$ coordination common for copper oxysalt minerals. Cu2 and Cu6 atoms have almost planar square coordination. Cu5 atom demonstrates Jahn-Teller distorted octahedral coordination environments typical for Cu^{2+} cations.

There are two symmetrically independent tetrahedral T sites. The P/As ratio was refined for the $T1$ site, and it is in good agreement with the microprobe data. The $T1$ site is predominantly occupied by P^{5+} cations (Table 3). The $T2$ site is occupied by S^{6+} cations.

Microprobe analysis indicates the presence of a minor admixture of Si and V. However, those could not be refined. Average $\langle T1-O \rangle$ and $\langle T2-O \rangle$ bond-length values (Table 4) in karlditmarite correlate well with assigned cationic composition.

O3 to O9 oxygen atoms are bonded in TO_4 tetrahedra. O1 and O2 sites belong to additional oxygen atoms (Krivovichev et al. 2013) being tetrahedrally coordinated by four Cu atoms each (Figure 3). The O1 atom is tetrahedrally coordinated by Cu2, Cu3, Cu4 and Cu5 atoms thus forming an $O1Cu_4$ oxocentered tetrahedron. Similarly, the O2 atom is central in $O2Cu_4$ tetrahedron with two Cu1, one Cu4 and one Cu6 in the vertices. The average $\langle O1-Cu \rangle$ and $\langle O2-Cu \rangle$ bond lengths in karlditmarite are 1.922 and 1.941 Å, respectively. Both values are in good agreement with the typical $\langle O-Cu \rangle$ bond length in oxocentered OCu_4 tetrahedra (Filatov et al. 1992).

Two distinct views can be employed to describe the crystal structure of karlditmarite. According to a classical approach, the structure is built up of cation-centered copper polyhedra that share vertices to form a complex framework (Figure 4a). Framework cavities contain rows of isolated tetrahedra (along [100] and [001]) that share oxygen atoms with Cu-centered polyhedra. The crystal structure of karlditmarite is characterized by the tetrahedra arranged in layers, with layers of phosphate tetrahedra alternating with layers of sulfate tetrahedra (Figure 4b). The layers are parallel to the (001) plane. An alternative method is to use OCu_4 oxocentered tetrahedra to characterize the mineral structure. The cation-centered CuO_n polyhedra depicted in Figure 3 are variable and less rigid than OCu_4 oxocentered tetrahedra. Moreover, this method allows us to ascertain the position of karlditmarite in the structural classification of fumarolic minerals by contrasting its structural architecture with that of other copper oxysalt minerals and synthetic compounds.

The crystal structure of karlditmarite exhibits two distinct types of OCu_4 tetrahedra connectivities. $O1Cu_4$ tetrahedra share one vertex with $O2Cu_4$ tetrahedra (Figure 5a) and with each other via Cu5, Cu2, and Cu4 vertices, while the Cu3 vertex is free. An alternative scenario is

observed for the O_2Cu_4 tetrahedra. [Figure 5a](#) illustrates that, in addition to the corner sharing via Cu_4 and Cu_6 vertices, there is an extra $Cu_1 \dots Cu_1$ edge-sharing that results in the formation of ${}_{\infty}^0 [Cu_6O_2]^{8+}$ dimers. The topology of the resulting corrugated ${}_{\infty}^2 [Cu_9O_4]^{10+}$ layer parallel to (011) in karlditmarite is unique and has not been described previously in minerals and synthetic compounds. However, the layer can be split into two distinct types of chains ([Figure 5a](#)), which are frequently observed in fumarolic minerals. For example, fumarolic copper sulfates, such as kamchatkite, $KCu_3O(SO_4)_2Cl$ ([Siidra et al. 2017](#)) and vergasovaite, $Cu_3O(SO_4)(MoO_4)$ ([Nazarchuk et al. 2024](#)), copper selenite, chloromenite, $Cu_9O_2(SeO_3)_4Cl_6$ ([Vergasova et al. 1999](#)), and copper vanadate, yaroshevskite, $Cu_9O_2(VO_4)_4Cl_2$ ([Pekov et al. 2013](#); [Siidra et al. 2020](#)), are examples of crystal structures based on single ${}_{\infty}^1 [Cu_3O]^{4+}$ chains identical to those formed by O_1Cu_4 tetrahedra. Georgbokiite, $Cu_5O_2(SeO_3)_2Cl_2$ ([Krivovichev et al., 1999](#)) and antipovite, $Cu_5O_2(PO_4)_2$ ([Siidra et al. 2022](#)) are examples of fumarolic minerals structurally based on ${}_{\infty}^1 [Cu_5O_2]^{6+}$ chains that involve edge-sharing. The layer in karlditmarite can also be described as composed of six-membered rings ([Figure 5a](#)), in which two of the six tetrahedra share a common edge. The interlayer space between the bends of the highly corrugated ${}_{\infty}^2 [Cu_9O_4]^{10+}$ layers hosts phosphate tetrahedra, whereas sulfate tetrahedra are placed above the centers of the rings. ([Figure 6](#)).

4. Discussion

Recently, layers with ${}_{\infty}^2 [A_9O_4]^{10+}$ ($A = Cu^{2+}, Pb^{2+}$) distinct topologies were reported in vasilseverginite, $Cu_9O_4(AsO_4)_2(SO_4)_2$ ([Pekov et al. 2021](#)), and synthetic $[Cu^{2+}_6Pb_3O_4](Cu^+Pb_{1.27}Br_{3.54})(SeO_3)_4Br_2$ ([Siidra et al. 2018](#)) ([Figure 6b,c](#)). The latter was prepared through the chemical gas transport method, which emulates the formation of copper oxysalts in fumaroles with highly oxidizing environments. Two symmetrically independent but heterometallic $OPbCu_3$ tetrahedra are present in the crystal structure of the synthetic Pb-Cu selenite. The

topological function of the $O1PbCu_3$ tetrahedron is the same as that of the $O1Cu_4$ in the karlditmarite structure. The divalent lead cation with “lone pair” occupies a free vertex in $O1PbCu_3$ that is “raised” above the layer plane, while the other three vertices of the tetrahedron are shared with the neighboring ones. The stepped appearance of the $[A_9O_4]^{10+}$ layer in Pb-Cu selenite can be explained by this circumstance. Additionally, the topological function of the $O2Cu_4$ tetrahedron in the karlditmarite structure is the same as that of the $O2PbCu_3$ tetrahedron. Two $O2PbCu_3$ tetrahedra share a common edge to form the ${}^0_{\infty}[Cu_6O_2]^{8+}$ dimer (Figure 5b). Unlike in karlditmarite, the layer in synthetic Pb-Cu selenite can be split into only one type of chain that is topologically identical to that one formed by $O1Cu_4$ in karlditmarite and observed in a number of fumarolic minerals mentioned above. Meanwhile, the Pb-Cu selenite structure shows two distinct types of six-membered rings (Figure 5b).

${}^2_{\infty}[Cu_9O_4]^{10+}$ layer in the structure of vasilseverginite (Pekov et al. 2021) can also be described as consisting of ${}^0_{\infty}[Cu_6O_2]^{8+}$ dimers (Figure 5c). However, the topological function of all OCu_4 tetrahedra is the same. Each tetrahedron has one common edge and one common vertex with its two neighbors, respectively. Thus, the layer in vasilseverginite has a different structural topology than that in karlditmarite. The substantial difference in the size of the arsenate (in vasilseverginite) and phosphate (in karlditmarite) tetrahedral groups is the most probable explanation for the difference of the copper-oxide substructure in both minerals. The ${}^2_{\infty}[Cu_9O_4]^{10+}$ layers in the vasilseverginite structure are almost flat, while the ${}^2_{\infty}[Cu_9O_4]^{10+}$ layers in the karlditmarite structure are strongly corrugated because of the zig-zag form of the chains formed by the $O1Cu_4$ tetrahedra. Therefore, the karlditmarite structure is a novel structure type that has not been previously identified in synthetic compounds and minerals.

The abundance of anhydrous sulfates and the extraordinary rarity of copper phosphates in active volcanic fumaroles can be attributed to the well-known chalcophile nature of copper. Nevertheless, active volcanic fumaroles have been reported to contain phosphate minerals. Rare

apatite, as inclusions in magnetite, was mentioned as part of volcanic fragmentation aerosol (unaltered fragments of silicate melt and phenocrysts) by [Zelenski et al. \(2020\)](#); they also identified two unknown phases with approximate compositions “(Al,Fe)(PO₄)” and “(Na,K)(PO₄)” as secondary minerals in alteration aerosol (silicate particles altered by gases), and fluorapatite and goryainovite as minerals of unclear or nonvolcanic origin.

Volcanic gases can transport various trace elements, including P, in form of (i) gaseous complexes, (ii) liquid or solid aerosols (suspended in a gas flow), and (iii) solid particles produced by wall-rock disintegration by a gas or a chemical reaction between gas and wall-rock ([Wahrenberger et al. 2002](#); [Taran et al. 2018](#); [Zelenski et al. 2020, 2021](#)). Experimental study by [Yamagata et al. \(1991\)](#) suggest that P can originally be in form of P₄O₁₀ in high-temperature volcanic gases, and upon cooling, due to hydrolysis, P₄O₁₀ transforms to ortho-, pyro- and tripolyphosphates. The study of Mt. Usu (Japan) gases and thermodynamic calculations show that a predominant state of P in gases can be in form of PO₂ ([Mambo et al. 1991](#)).

Local enrichment of a volcanic gas (or gas condensate) in P can be a result of gas-basaltic rock interaction, e.g. during “gas metasomatism” process and formation of incrustation and/or sublimate / exhalative minerals ([Borisov et al. 2024](#); [Bulakh et al. 2024b](#)) or dispersed rock aerosol ([Taran et al. 2018](#)). Phosphorus is a minor component in Tolbachik basalts; the element content in whole-rock samples reach 0.8 wt% P₂O₅, but typically is up to 0.6 wt% ([Churikova et al. 2015](#)). Slightly higher P content is detected in groundmass glass: up to 1.0 wt% P₂O₅ ([Borisov et al. 2024](#), [Bulakh et al. 2024a](#)). We suggest that P can be liberated due to the local and small-scale interaction between hot water-rich gases and alkali-bearing silicate glass, and can be fixed in secondary minerals after primary basaltic minerals (e.g. secondary olivine with up to 0.7 wt% P₂O₅, [Borisov et al. 2024](#)), metasomatic minerals (e.g. sanidine with up to 2.0 wt% P₂O₅, [Bulakh et al. 2024b](#)), and sublimate minerals (e.g. fluorapatite).

Implications

The discovery of karlditmarite confirms the potential for the formation of anhydrous mixed copper sulfate-phosphates in active fumaroles. Copper phosphates have not been previously identified in the fumaroles of the Tolbachik volcano scoria cones, despite the presence of nearly a hundred distinct copper oxides and oxysalts. Rare occurrence of P-bearing and phosphate minerals in Tolbachik fumaroles can be explained by extremely low P content in fumarolic gases (230 ± 210 ppb, [Zelenski et al. 2014](#)) and gas condensates (61-71 ppb, [Chaplygin et al. 2016](#)). Low P content is also detected in gas condensate from the active Gorely volcano, southern Kamchatka (106 ppb, [Chaplygin et al. 2015](#)) and Pallas volcano, Kuril Island arc (8-23 ppb, [Taran et al. 2018](#)). In contrast, fumarolic condensate from Kudryavy volcano (Kuril Island arc) contains much higher P, between 0.2 and 30.8 ppm ([Taran et al. 1995](#)), however, recent study of high-temperature condensate also revealed a very low P content (56 ppb, [Taran et al. 2018](#)). Enrichment factor for P (normalized to Mg) for condensates from both Pallas and Kudryavy volcanoes are low (0.3-0.8 and 1.05 respectively), and the patterns of trace and rock-forming elements distribution (expressed as enrichment factor) are similar to that for high-temperature gas condensates from other localities ([Taran et al. 2018](#)). Apparent partition coefficient Kd^* for P in volcanic gas – silicate melt system (for arc tectonic setting) is extremely low (0.00016; [Zelenski et al. 2021](#)), and this explains low P content in gas condensate.

Minerals that contain tetrahedral divalent copper complexes are an exceptional source of inspiration and playground for the investigation of intricate magnetic phenomena (e.g. [Tang et al. 2016](#); [Nekrasova et al. 2020](#); [Biesner et al. 2022](#); [Ginga et al. 2024](#)). The layer in the crystal structure of karlditmarite contains $\frac{1}{\infty}[\text{Cu}_3\text{O}]^{4+}$ chains. Several intriguing magnetic phenomena were found when frustrated magnets, such as kamchatkite ([Volkova and Marinin, 2018](#)) and yaroshevskite ([Siidra et al. 2020](#)), with similar chain structures, were examined. The copper-oxide substructure of karlditmarite is significantly complicated by the presence of $\frac{1}{\infty}[\text{Cu}_5\text{O}_2]^{6+}$ chains in addition to the $\frac{1}{\infty}[\text{Cu}_3\text{O}]^{4+}$ chains. The six-membered ring topology observed in karlditmarite can

be also regarded as distorted and highly frustrated capped kagome layers, as exemplified by averievite (Korniyakov et al. 2021), but with a "defect" where one of the connections between OCu_4 tetrahedra occurs via edge-sharing rather than corner-sharing. Recently, there has been a significant increase in interest in synthetic averievites in the field of magnetic phenomena (e.g. Botana et al. 2018; Guchhait et al. 2024; Liu et al. 2024). Consequently, a thorough magnetic investigation of a pure synthetic analogue of the mineral would be highly beneficial. The $\text{Cu}\cdots\text{Cu}$ contact values in karlditmarite fluctuate between 2.93 to 3.35 Å (O1Cu_4) and 2.85 to 3.41 Å (O2Cu_4). Nevertheless, the microscopic magnetic models are frequently rather complex and significantly distinct from the simple interaction schemes that can be deduced from the geometrical arrangement of the Cu atoms in the crystal structure. Studies of the quantum magnetism in the karlditmarite synthetic analogue are currently in progress.

Acknowledgements

We acknowledge Tonči Balić-Žunić and two anonymous reviewers for their comments that improved the manuscript. This work was financially supported by the Russian Science Foundation through the grant 25-17-00157. We also acknowledge the Library of the Russian Academy of Sciences as well as the Library of the University of Kiel for providing the repository materials used in Figure 1. The technical support by the St. Petersburg State University X-ray Diffraction Resource Center is acknowledged.

References

1. Belousov, A., Belousova, M., Edwards, B., Volynets, A., and Melnikov, D. (2015) Overview of the precursors and dynamics of the 2012–13 basaltic fissure eruption of Tolbachik Volcano, Kamchatka, Russia. *Journal of Volcanology and Geothermal Research*, 307, 22–37. <https://doi.org/10.1016/j.jvolgeores.2015.06.013>
2. Biesner, T., Roh, S., Pustogow, A., Zheng, H., Mitchell, J.F., and Dressel, M. (2022) Magnetic terahertz resonances above the Néel temperature in the frustrated kagome antiferromagnet averievite. *Physical Reviews B*, 105, L060410. <https://doi.org/10.1103/PhysRevB.105.L060410>
3. Borisov, A.S., Siidra, O.I., Vlasenko, N.S., Platonova, N.V., Schuldt, T., Neuman, M., Strauss, H., and Holzheid, A. (2024) The Yadovitaya fumarole, Tolbachik volcano: A comprehensive mineralogical and geochemical study and driving factors for mineral diversity. *Geochemistry*, 84, 126179. <https://doi.org/10.1016/j.chemer.2024.126179>
4. Botana, A.S., Zheng, H., Lapidus, S.H., Mitchell, J.F., Norman, M.R. (2018) Averievite: A copper oxide kagome antiferromagnet. *Physical Review*, B98, 054421. <https://doi.org/10.1103/PhysRevB.98.054421>
5. Bulakh, M.O., Pekov, I.V., Koshlyakova, N.N., and Nazarova, M.A. (2024a) Basalt alteration in high-temperature oxidizing-type fumaroles at the Tolbachik volcano (Kamchatka, Russia). Part 1: Processes and products of olivine alteration. *Geology of Ore Deposits*, 66, 1057–1082. <https://doi.org/10.1134/S1075701524700235>
6. Bulakh, M.O., Pekov, I.V., Koshlyakova, N.N., and Nazarova, M.A. (2024b) Basalt alteration in high-temperature oxidizing-type fumaroles at the Tolbachik volcano (Kamchatka, Russia). Part 2: Gas metasomatites. *Geology of Ore Deposits*, 66, 1083–1122. <https://doi.org/10.1134/S1075701524700259>
7. Chaplygin, I.V., Taran, Yu.A., Dubinina, E.O., Shapar, V.N., and Timofeeva, I.F. (2015) Chemical composition and metal capacity of magmatic gases of Gorelyi volcano,

Kamchatka. Doklady Earth Sciences, 463, 690–694.

<https://doi.org/10.1134/S1028334X15050104>

8. Chaplygin, I.V., Lavrushin, V.Y., Dubinina, E.O., Bychkova, Y.V., Inguaggiato, S., and Yudovskaya, M.A. (2016) Geochemistry of volcanic gas at the 2012–13 New Tolbachik eruption, Kamchatka. *Journal of Volcanology and Geothermal Research*, 323, 186–193.
<https://doi.org/10.1016/j.jvolgeores.2016.04.005>
9. Churikova, T.G., Gordeychik, B.N., Edwards, B.R., Ponomareva, V.V., and Zelenin, E.A. (2015) The Tolbachik volcanic massif: A review of the petrology, volcanology and eruption history prior to the 2012–2013 eruption. *Journal of Volcanology and Geothermal Research*, 307, 3–21. <https://doi.org/10.1016/j.jvolgeores.2015.10.016>
10. Ditmar, C.v. (1856) Ein Paar erläuternde Worte zur geognostischen Karte Kamtschatka's (mit einer Karte). *Bulletin de la Classe physico-mathématique de l'Académie impériale des sciences de Saint-Petersbourg*, 14, 241–250.
11. Ditmar, C.v. (1860) Die Vulkane und heissen Quellen Kamtschatka's. *Mittheilungen aus Justus Perthes' Geographischer Anstalt über wichtige neue Erforschungen auf dem Gesamtgebiete der Geographie*, 6, 66–67.
12. Ditmar, C.v. (1890) *Reisen und Aufenthalt in Kamtschatka in den Jahren 1851–1855*. Erster Teil, 867 p. St. Petersburg.
13. Fedotov, S.A. and Markhinin, Y.K., Eds. (1984) *The Great Tolbachik Fissure Eruption*. 341 p. Cambridge University Press, New York.
14. Gagné, O.C., and Hawthorne, F.C. (2015) Comprehensive derivation of bond-valence parameters for ion pairs involving oxygen. *Acta Crystallographica*, B71, 562–578.
<https://doi.org/10.1107/S2052520615016297>
15. Ginga, V.A., Siidra, O.I., Tsirlin, A.A., and Setzer, A. (2024) Assembling the puzzle of coparsite polymorphism: synthesis, thermal expansion, and quantum magnetism of α - and

β -Cu₄O₂(VO₄)Cl. Inorganic Chemistry, 63, 24573–24586.

<https://doi.org/10.1021/acs.inorgchem.4c03694>

16. Guchhait, S., Ambika, D.V., Mohanty, S., Furukawa, Y. and Nath, R. (2024) Magnetic properties of the frustrated spin-12 capped-kagome antiferromagnet (CsBr)Cu₅V₂O₁₀. Physical Review, B110, 174447. <https://doi.org/10.1103/PhysRevB.110.174447>
17. Korniyakov, I.V., Vladimirova, V.A., Siidra, O.I. and Krivovichev, S.V. (2021) Expanding the averievite family, (MX)Cu₅O₂(T⁵⁺O₄)₂ (T⁵⁺ = P, V; M = K, Rb, Cs, Cu; X = Cl, Br): synthesis and single-crystal X-ray diffraction study. Molecules, 26, 1833. <https://doi.org/10.3390/molecules26071833>
18. Koshlyakova, N.N., Pekov, I.V., Vigasina, M.F., Agakhanov, A.A., and Nazarova, M.A. (2022) A novel solid solution between wagnerite and arsenowagnerite. Doklady Earth Sciences, 507, 900–903. <https://doi.org/10.1134/S1028334X22700404>
19. Krivovichev, S.V., Shuvalov, R.R., Semenova, T.F., and Filatov, S.K. (1999) Crystal chemistry of inorganic compounds based on chains of oxocentered tetrahedra. III. Crystal structure of georgbokiite, Cu₅O₂(SeO₃)₂Cl₂. Zeitschrift für Kristallographie, 214, 135–138. <https://doi.org/10.1524/zkri.1999.214.3.135>
20. Krivovichev, S.V., Mentré, O., Siidra, O.I., Colmont, M., and Filatov, S.K. (2013) Anion-centered tetrahedra in inorganic compounds. Chemical Reviews, 113, 6459–6535. <https://doi.org/10.1021/cr3004696>.
21. Liu, C., Chang, T., Wang, S., Zhou, S., Wang, X., Fan, C., Han, L., Li, F., Ren, H., Wang, S., Chen, Y.-S. and Zhang, J. (2024) Cascade of phase transitions and large magnetic anisotropy in a triangle-kagome-triangle trilayer antiferromagnet. Chemistry of Materials, 36, 9516 - 9525. <https://doi.org/10.1021/acs.chemmater.4c01342>
22. Mambo, V.S., Yoshida, M., and Matsuo, S. (1991) Partition of arsenic and phosphorus between volcanic gases and rock. Part I: analytical data and magmatic conditions of Mt.

- Usu, Japan. *Journal of Volcanology and Geothermal Research*, 46, 37–47.
[https://doi.org/10.1016/0377-0273\(91\)90074-A](https://doi.org/10.1016/0377-0273(91)90074-A)
23. Menyailov, I.A., and Nikitina, L.P. (1980) Chemistry and metal contents of magmatic gases: the new Tolbachik volcanoes case (Kamchatka). *Bulletin of Volcanology*, 43, 195–205. <https://doi.org/10.1007/BF02597621>
24. Nazarchuk, E.V., Siidra, O.I., Charkin, D.O., Nikolaevich, G.V., Borisov, A.S., and Ugolkov, V.L. (2024) Vergasovaite to cupromolybdate topotactic transformation with crystal shape preservation. *American Mineralogist*, 109, 471–481.
<https://doi.org/10.2138/am-2022-8753>
25. Nekrasova, D.O., Tsirlin, A.A., Colmont, M., Siidra, O.I., Vezin, H., and Mentré, O. (2020) Magnetic hexamers interacting in layers in the $(\text{Na,K})_2\text{Cu}_3\text{O}(\text{SO}_4)_3$ minerals. *Physical Reviews B*, 102, 184405. <https://doi.org/10.1103/PhysRevB.102.184405>
26. Pekov, I.V., Zubkova, N.V., Zelenski, M.E., Yapaskurt, V.O., Polekhovskiy, Yu.S., Fadeeva, O.A., and Pushcharovskiy, D.Yu. (2013) Yaroshevskite, $\text{Cu}_9\text{O}_2(\text{VO}_4)_4\text{Cl}_2$, a new mineral from the Tolbachik volcano, Kamchatka, Russia. *Mineralogical Magazine*, 77, 107–116. <https://doi.org/10.1180/minmag.2013.077.1.10>
27. Pekov, I.V., Agakhanov, A.A., Zubkova, N.V., Koshlyakova, N.N., Shchipalkina, N.V., Sandalov, F.D., Yapaskurt, V.O., Turchkova, A.G., and Sidorov, E.G. (2020) Oxidizing-type fumaroles of the Tolbachik volcano, a mineralogical and geochemical unique. *Russian Geology and Geophysics*, 61, 675–688. <https://doi.org/10.15372/RGG2019167>
28. Pekov, I.V., Britvin, S.N., Krivovichev, S.V., Yapaskurt, V.O., Vigasina, M.F., Turchkova, A.G., and Sidorov, E.G. (2021) Vasilseverginite, $\text{Cu}_9\text{O}_4(\text{AsO}_4)_2(\text{SO}_4)_2$, a new fumarolic mineral with a hybrid structure containing novel type of anion-centered tetrahedral structural units. *American Mineralogist*, 106, 633–640.
<https://doi.org/10.2138/am-2020-7611>

29. Pekov, I.V., Koshlyakova, N.N., Zubkova, N.V., Krz̄ała, A., Belakovskiy, D.I., Galuskina, I.O., Galuskin, E.V., Britvin, S.N., Sidorov, E.G., Vapnik, Y., and Pushcharovsky, D.Yu. (2022) Pliniusite, $\text{Ca}_5(\text{VO}_4)_3\text{F}$, a new apatite-group mineral and the novel natural ternary solid-solution system pliniusite–svabite–fluorapatite. *American Mineralogist*, 107, 1626–1634. <https://doi.org/10.2138/am-2022-8100>
30. Pekov, I.V., Zubkova, N.V., Agakhanov, A.A., Turchkova, A.G., Zhitova, E.S., and Pushcharovskii, D.Yu. (2023) A new chladniite variety from volcanic exhalations. The genetic crystal chemistry of chladniite. *Doklady Earth Sciences*, 512, 975–982. <https://doi.org/10.1134/S1028334X23601591>
31. Sheldrick, G. M. (2015). SHELXT – Integrated space-group and crystal-structure determination. *Acta Crystallographica*, 71, 3–8. <https://doi.org/10.1107/S2053273314026370>
32. Shchipalkina, N.V., Pekov, I.V., Zubkova, N.V., Koshlyakova, N.N., and Sidorov, E.G. (2019) Natural forsterite strongly enriched by arsenic and phosphorus: chemistry, crystal structure, crystal morphology and zonation. *Physics and Chemistry of Minerals*, 46, 889–898. <https://doi.org/10.1007/s00269-019-01048-8>
33. Shchipalkina, N.V., Pekov, I.V., Koshlyakova, N.N., Britvin, S.N., Zubkova, N.V., Varlamov, D.A., and Sidorov, E.G. (2020a) Unusual silicate mineralization in fumarolic sublimates of the Tolbachik volcano, Kamchatka, Russia – Part 1: Neso-, cyclo-, ino- and phyllosilicates. *European Journal of Mineralogy*, 32, 101–119. <https://doi.org/10.5194/ejm-32-101-2020>
34. Shchipalkina, N.V., Pekov, I.V., Koshlyakova, N.N., Britvin, S.N., Zubkova, N.V., Varlamov, D.A., and Sidorov, E.G. (2020b) Unusual silicate mineralization in fumarolic sublimates of the Tolbachik volcano, Kamchatka, Russia – Part 2: Tectosilicates. *European Journal of Mineralogy*, 32, 121–136. <https://doi.org/10.5194/ejm-32-121-2020>

35. Shchipalkina, N.V., Pekov, I.V., Britvin, S.N., Koshlyakova, N.N., and Sidorov, E.G. (2020c) Arsenic and phosphorus in feldspar framework: sanidine–filatovite solid-solution series from fumarolic exhalations of the Tolbachik volcano, Kamchatka, Russia. *Physics and Chemistry of Minerals*, 47, 1. <https://doi.org/10.1007/s00269-019-01067-5>
36. Siidra, O.I., Nazarchuk, E.V., Zaitsev, A.N., Lukina, E.A., Avdontseva, E.Y., Vergasova, L.P., Vlasenko, N.S., Filatov, S.K., Turner, R., and Karpov, G.A. (2017) Copper oxosulphates from fumaroles of Tolbachik Vulcano: Puninite, $\text{Na}_2\text{Cu}_3\text{O}(\text{SO}_4)_3$ – a new mineral species and structure refinements of kamchatkite and alumoklyuchevskite. *European Journal of Mineralogy*, 29, 499–510. <https://doi.org/10.1127/ejm/2017/0029-2619>
37. Siidra, O.I., Kozin, M.S., Depmeier, W., Kayukov, R.A., and Kovrugin, V.M. (2018) Copper – lead selenite bromides: A new large family of compounds partly having Cu^{2+} substructures derivable from Kagome-nets. *Acta Crystallographica*, B74, 712–724. <https://doi.org/10.1107/S2052520618016542>
38. Siidra, O.I., Vladimirova, V.A., Tsirlin, A.A., Chukanov, N.V., and Ugolkov, V.L. (2020) $\text{Cu}_9\text{O}_2(\text{VO}_4)_4\text{Cl}_2$, the first copper oxychloride vanadate: mineralogically inspired synthesis and magnetic behavior. *Inorganic Chemistry*, 59, 2136–2143. <https://doi.org/10.1021/acs.inorgchem.9b02565>
39. Siidra, O.I., Nazarchuk, E.N., Pautov, L.A., Borisov, A.S., Zaitsev, A.N., Avdontseva, E.Y. and Bocharov, V.N. (2021) Paulgrothite, IMA 2021-004. *CNMNC Newsletter* 64; *Mineralogical Magazine*, 85, <https://doi.org/10.1180/mgm.2021.93>
40. Siidra, O.I., Nazarchuk, E.V., Pautov, L.A., Borisov, A.S., Mirakov, M.A. (2022) Antipovite, IMA 2022-064, In *CNMNC Newsletter* 70. *European Journal of Mineralogy*, 34. <https://doi.org/10.5194/ejm-34-591-2022>

41. Siidra, O. I., Nazarchuk, E. V., Pautov, L. A., Borisov, A. S., and Kozin, M. S. (2021b) Milkovoite, IMA 2021-005, in: CNMNC Newsletter 61, European Journal of Mineralogy, 33, <https://doi.org/10.5194/ejm-33-299-2021>, 2021.
42. Tang, Y., Guo, W., Zhang, S., Xiang, H., Cui, M., and He, Z. (2016) $\text{Na}_2\text{Cu}_7(\text{SeO}_3)_4\text{O}_2\text{Cl}_4$: a selenite chloride compound with Cu_7 units showing spin-frustration and a magnetization plateau. Dalton Transactions, 45, 8324–8326. <https://doi.org/10.1039/C6DT01120A>
43. Taran, Yu.A., Hedenquist, J.W., Korzhinsky, M.A., Tkachenko, S.I., and Shmulovich K.I. (1995) Geochemistry of magmatic gases from Kudryavy volcano, Iturup, Kuril Islands. Geochimica et Cosmochimica Acta, 59, 1749–1761. [https://doi.org/10.1016/0016-7037\(95\)00079-F](https://doi.org/10.1016/0016-7037(95)00079-F)
44. Taran, Y., Zelenski, M., Chaplygin, I., Malik, N., Champion, R., Inguaggiato, S., Pokrovsky, B., Kalacheva, E., Melnikov, D., Kazahaya, R. and Fischer, T. (2018) Gas emissions from volcanoes of the Kuril Island arc (NW Pacific): Geochemistry and fluxes. Geochemistry, Geophysics, Geosystems, 19, 1859–1880. <https://doi.org/10.1029/2018GC007477>
45. Vergasova, L.P., and Filatov, S.K. (1993) Volcanic exhalative minerals, a specific genetic group (from data on the 1975–1976 Tolbachik eruption). Proceedings of the All-Union Mineralogical Society, 122, 68–76 (In Russian).
46. Vergasova, L., Krivovichev, S., Semenova, T., Filatov, S., and Ananiev, V. (1999) Chloromenite, $\text{Cu}_9\text{O}_2(\text{SeO}_3)_4\text{Cl}_6$, a new mineral from the Tolbachik volcano, Kamchatka, Russia. European Journal of Mineralogy, 11, [119–124](https://doi.org/10.1127/ejm/11/1/0119). <https://doi.org/10.1127/ejm/11/1/0119>
47. Vergasova, L.P., and Filatov, S.K. (2016) A study of volcanogenic exhalation mineralization. Journal of Volcanology and Seismology, 10, 71–85. <https://doi.org/10.1134/S0742046316020068>

48. Volkova, L.M., and Marinin, D.V. (2018) Spin-frustrated pyrochlore chains in the volcanic mineral kamchatkite ($\text{KCu}_3\text{OCl}(\text{SO}_4)_2$). *Physics and Chemistry of Minerals*, 45, 655–668. <https://doi.org/10.1007/s00269-018-0950-5>
49. Wahrenberger, C., Seward, T.M., and Dietrich, V. (2002) Volatile trace-element transport in high-temperature gases from Kudriavy volcano (Iturup, Kurile Islands, Russia). In R. Hellmann, S.A. Wood, Eds., *Water-Rock Interactions, Ore Deposits, and Environmental Geochemistry*, The Geochemical Society Special Publication No.7, p. 307–327.
50. Yamagata, Y., Watanabe, H., Saitoh, M., and Namba, T. (1991) Volcanic production of polyphosphates and its relevance to prebiotic evolution. *Nature*, 352, 516–519. <https://doi.org/10.1038/352516a0>
51. Zelenski, M., Malik, N., and Taran, Y. (2014) Emissions of trace elements during the 2012–2013 effusive eruption of Tolbachik volcano, Kamchatka: Enrichment factors, partition coefficients and aerosol contribution. *Journal of Volcanology and Geothermal Research*, 285, 136–149. <https://doi.org/10.1016/j.jvolgeores.2014.08.007>
52. Zelenski, M., Kamenetsky, V.S., Taran, Y., and Kovalskii, A.M. (2020) Mineralogy and origin of aerosol from an arc basaltic eruption: Case study of Tolbachik volcano, Kamchatka. *Geochemistry, Geophysics, Geosystems*, 21, e2019GC008802. <https://doi.org/10.1029/2019GC008802>
53. Zelenski, M., Simakin, A., Taran, Yu., Kamenetsky, V.S. and Malik, N. (2021) Partitioning of elements between high-temperature, low-density aqueous fluid and silicate melt as derived from volcanic gas geochemistry. *Geochimica et Cosmochimica Acta*, 295, 112–134. <https://doi.org/10.1016/j.gca.2020.12.011>

List of Figure captions:

Figure 1. «Reisen und Aufenthalt in Kamtschatka in den Jahren 1851–1855» (Travels and stay in Kamchatka in the years 1851–1855) title page (a) and an illustration of the Avacha Bay and

Koryaksky Volcano (b). A title page for the first geological ("geognostic") map of the Kamchatka Peninsula, which was compiled by Karl von Ditmar following his expeditions (enlarged text fragments are given in red frames) (c, d).

Figure 2. Well-shaped olive-green karlditmarite crystal in association with anhydrite and langbeinite (white and yellow), euchlorine (emerald-green) and tenorite (black).

Figure 3. Atom coordination environments in karlditmarite. Ellipsoids are given at 50% probability level.

Figure 4. General projection of the crystal structure of karlditmarite in polyhedral representation (CuO_n = blue, SO_4 = yellow, PO_4 = violet) (a). Highlighted pseudolayered arrangement of sulfate and phosphate tetrahedra (b).

Figure 5. ${}^2_{\infty}[\text{A}_9\text{O}_4]^{10+}$ ($A = \text{Cu}^{2+}, \text{Pb}^{2+}$) layers in minerals and synthetic compounds. General projection of the ${}^2_{\infty}[\text{Cu}_9\text{O}_4]^{10+}$ layer in the crystal structure of karlditmarite (a) (O1Cu₄ tetrahedra = red; O2Cu₄ tetrahedra = green; six-membered rings are highlighted in yellow). General projection of the ${}^2_{\infty}[\text{Cu}^{2+}_6\text{Pb}_3\text{O}_4]^{10+}$ layer in the crystal structure of $[\text{Cu}^{2+}_6\text{Pb}_3\text{O}_4](\text{Cu}^+\text{Pb}_{1.27}\text{Br}_{3.54})(\text{SeO}_3)_4\text{Br}_2$ (Siidra et al. 2018) (b) (O1PbCu₃ tetrahedra = red; O2PbCu₃ tetrahedra = green; two different six-membered rings are highlighted in colors). General projection of the ${}^2_{\infty}[\text{Cu}_9\text{O}_4]^{10+}$ layer in vasilsevergenite (Pekov et al. 2021) (c) (OCu₄ tetrahedra = green). See the text for details.

Figure 6. Polyhedral representation of the crystal structure of karlditmarite (O1Cu₄ tetrahedra = red; O2Cu₄ tetrahedra = green; SO_4 tetrahedra = yellow; PO_4 tetrahedra = violet).

Table 1. Analytical data (wt %) for karlditmarite.

Constituent	Mean	Range	Stand. Dev.	Probe Standard
CuO	65.57	63.2-67.55	0.52	Cu ₂ S
ZnO	1.36	0.43-1.93	0.13	ZnO
CaO	0.1	0.07-0.24	0.08	Wollastonite
Fe ₂ O ₃	1.2	0.67-1.7	0.33	Fe ₂ O ₃
Al ₂ O ₃	0.26	0.09-0.51	0.12	AlPO ₄
As ₂ O ₅	4.88	3.65-5.43	0.26	InAs
V ₂ O ₅	0.95	0.36-1.33	0.2	V ₂ O ₅
SiO ₂	0.34	0.12-0.53	0.15	Wollastonite
P ₂ O ₅	10.69	9.98-11.84	0.57	AlPO ₄
SO ₃	13.9	13.47-14.57	0.42	SrSO ₄
Total	99.25			

Table 2. Crystallographic data and refinement parameters for karlditmarite.

Crystal data	
Structural formula	Cu ₉ O ₄ (P _{0.797(5)} As _{0.203(5)} O ₄) ₂ (SO ₄) ₂
Space group	<i>P</i> -1
Unit cell dimensions <i>a</i> , <i>b</i> , <i>c</i> (Å)	6.1256(7), 7.9192(8), 7.9866(8)
α, β, γ (°)	75.173(2), 86.639(2), 88.660(2)
Unit-cell volume (Å ³)	373.87(7)
<i>Z</i>	1
Calculated density (g·cm ⁻³)	4.601
Absorption coefficient (mm ⁻¹)	14.004
Crystal size (mm)	0.02×0.02×0.10
Data collection	
Temperature (K)	293
Radiation, wavelength (Å)	MoK α , 0.71073
θ range (°)	2.642 – 29.573
<i>h</i> , <i>k</i> , <i>l</i> ranges	-8→5, -10→8, -10→11
Total reflections collected	3414
Unique reflections (<i>R</i> _{int})	1867 (0.044)
Unique reflections <i>F</i> > 4 σ (<i>F</i>)	1520
Structure refinement	
Refinement method	Full-matrix least-squares on <i>F</i> ²
Weighting coefficients <i>a</i> , <i>b</i>	0.054300, 0.361900
Data/restraints/parameters	1867/0/156
<i>R</i> ₁ [<i>F</i> > 4 σ (<i>F</i>)], <i>wR</i> ₂ [<i>F</i> > 4 σ (<i>F</i>)]	0.039, 0.092
<i>R</i> ₁ all, <i>wR</i> ₂ all	0.052, 0.097

Gof on F^2	1.034
Largest diff. peak and hole ($e \text{ \AA}^{-3}$)	1.811, -0.893

Table 3. Coordinates, isotropic displacement parameters (\AA^2) and bond-valence sums of atoms in karlditmarite.

Atom	<i>B.V.S.</i>	<i>Wyck. site</i>	<i>x</i>	<i>y</i>	<i>z</i>	<i>U_{eq}</i>
Cu1	2.00	2i	0.50705(12)	0.47599(10)	0.82910(9)	0.01043(19)
Cu2	1.94	1b	0	0	½	0.0094(2)
Cu3	1.99	2i	0.22200(13)	0.24068(10)	0.65685(10)	0.0155(2)
Cu4	1.91	2i	0.26839(12)	0.81348(10)	0.84937(10)	0.0143(2)
Cu5	2.10	1f	½	0	½	0.0099(2)
Cu6	1.82	1c	0	½	0	0.0107(2)
P1*	4.88	2i	0.74892(19)	0.35794(15)	0.51731(15)	0.0089(4)
S1	5.80	2i	-0.2480(2)	0.87153(19)	0.92419(18)	0.0094(3)
O1	2.07	2i	0.2327(7)	0.0016(5)	0.6451(5)	0.0089(8)
O2	1.95	2i	0.3010(7)	0.5706(5)	0.9746(5)	0.0093(8)
O3	2.13	2i	-0.0495(7)	0.7580(6)	0.9022(6)	0.0143(9)
O4	1.94	2i	0.5470(7)	0.2373(5)	0.5198(6)	0.0143(9)
O5	2.03	2i	0.0305(7)	0.7496(5)	0.4931(5)	0.0139(9)
O6	1.97	2i	0.5906(7)	0.8425(6)	0.8016(5)	0.0156(9)
O7	1.93	2i	0.2650(8)	0.4847(6)	0.6569(6)	0.0157(9)
O8	1.94	2i	0.3468(8)	0.1947(6)	0.8969(6)	0.0192(10)
O9	1.85	2i	0.7446(7)	0.4344(6)	0.6789(5)	0.0145(9)
O10	1.70	2i	-0.1836(8)	0.0515(6)	0.8895(7)	0.0250(11)

*P_{0.797(5)}As_{0.203(5)}.

Table 4. Selected interatomic distances (in \AA) in karlditmarite.

Cu1-O9	1.908(4)	Cu5-O1	1.951(4) ×2
Cu1-O2	1.933(4)	Cu5-O4	1.955(4) ×2
Cu1-O2	1.968(4)	Cu5-O6	2.500(4) ×2
Cu1-O7	2.069(4)		
Cu1-O8	2.375(5)	Cu6-O2	1.924(4) ×2
		Cu6-O3	2.015(4) ×2
Cu2-O1	1.891(4) ×2		
Cu2-O5	2.002(4) ×2	P1-O9	1.558(4)
		P1-O4	1.577(4)
Cu3-O1	1.919(4)	P1-O5	1.589(4)
Cu3-O7	1.957(4)	P1-O7	1.618(5)
Cu3-O5	1.999(4)	<P1-O>	1.586
Cu3-O8	2.048(4)		
Cu3-O4	2.218(5)	S1-O10	1.441(5)
		S1-O8	1.488(5)
Cu4-O1	1.927(4)	S1-O6	1.493(4)
Cu4-O2	1.939(4)	S1-O3	1.524(4)
Cu4-O6	1.996(4)	<S1-O>	1.487
Cu4-O3	2.003(4)		
Cu4-O10	2.598(5)		

Figures:



Figure 1. «Reisen und Aufenthalt in Kamtschatka in den Jahren 1851–1855» (Travels and stay in Kamchatka in the years 1851–1855) title page (a) and an illustration of the Avacha Bay and Koryaksky Volcano (b). A title page for the first geological ("geognostic") map of the Kamchatka Peninsula, which was compiled by Karl von Dittmar following his expeditions (enlarged text fragments are given in red frames) (c, d).

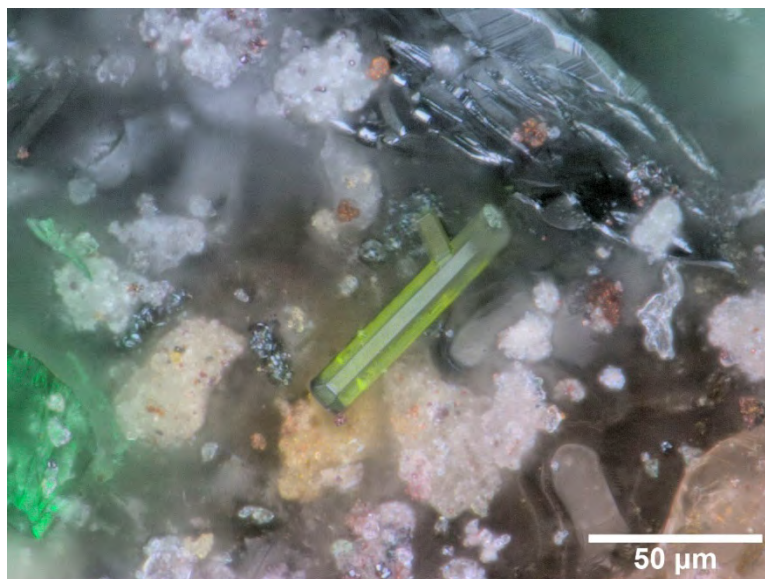


Figure 2. Well-shaped olive-green karlditmarite crystal in association with anhydrite and langbeinite (white and yellow), euchlorine (emerald-green) and tenorite (black).

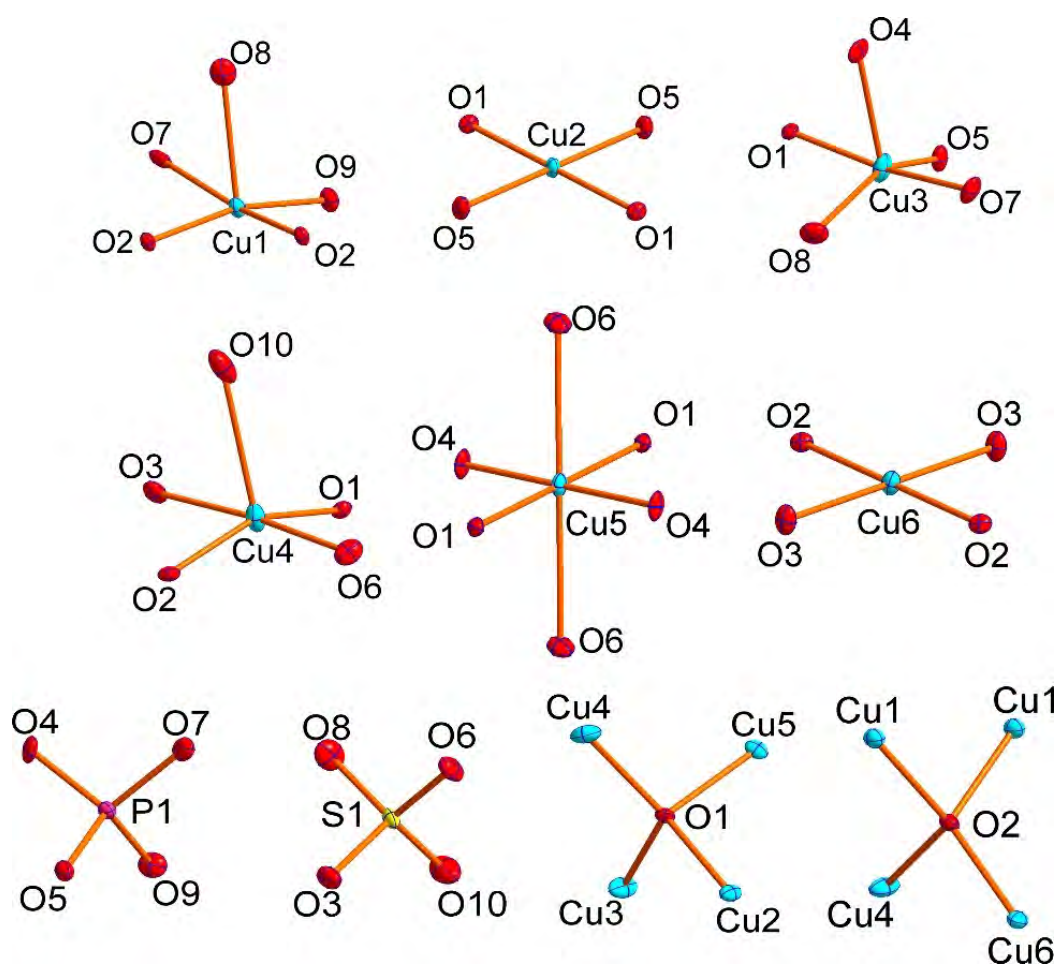


Figure 3. Atom coordination environments in karlditmarite. Ellipsoids are given at 50% probability level.

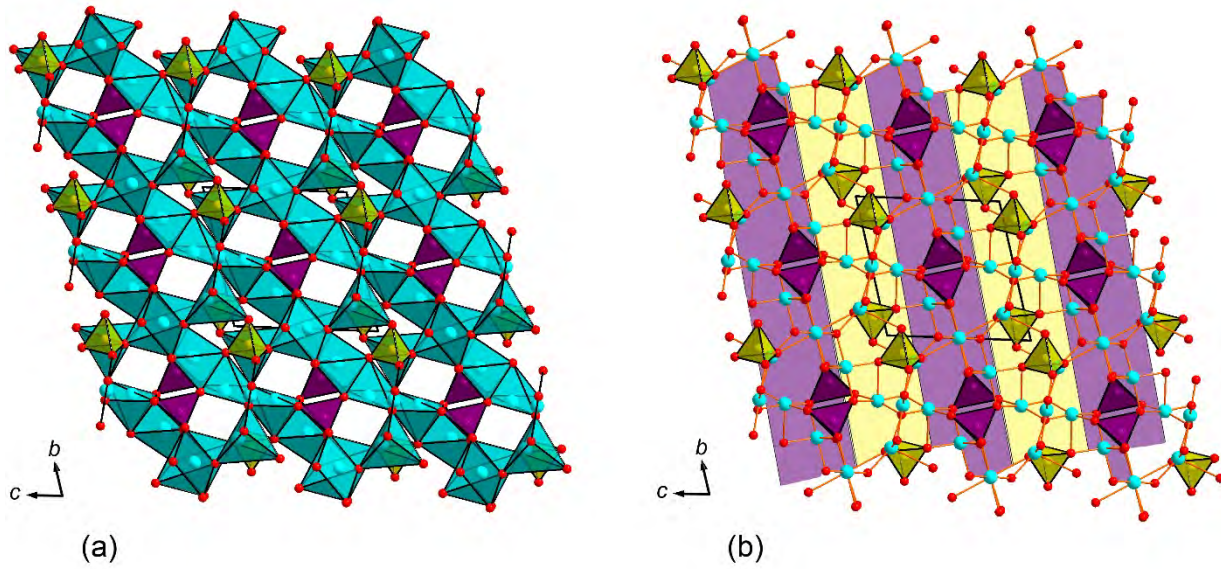


Figure 4. General projection of the crystal structure of karlditmarite in polyhedral representation (CuO_n = blue, SO_4 = yellow, PO_4 = violet) (a). Highlighted pseudolayered arrangement of sulfate and phosphate tetrahedra (b).

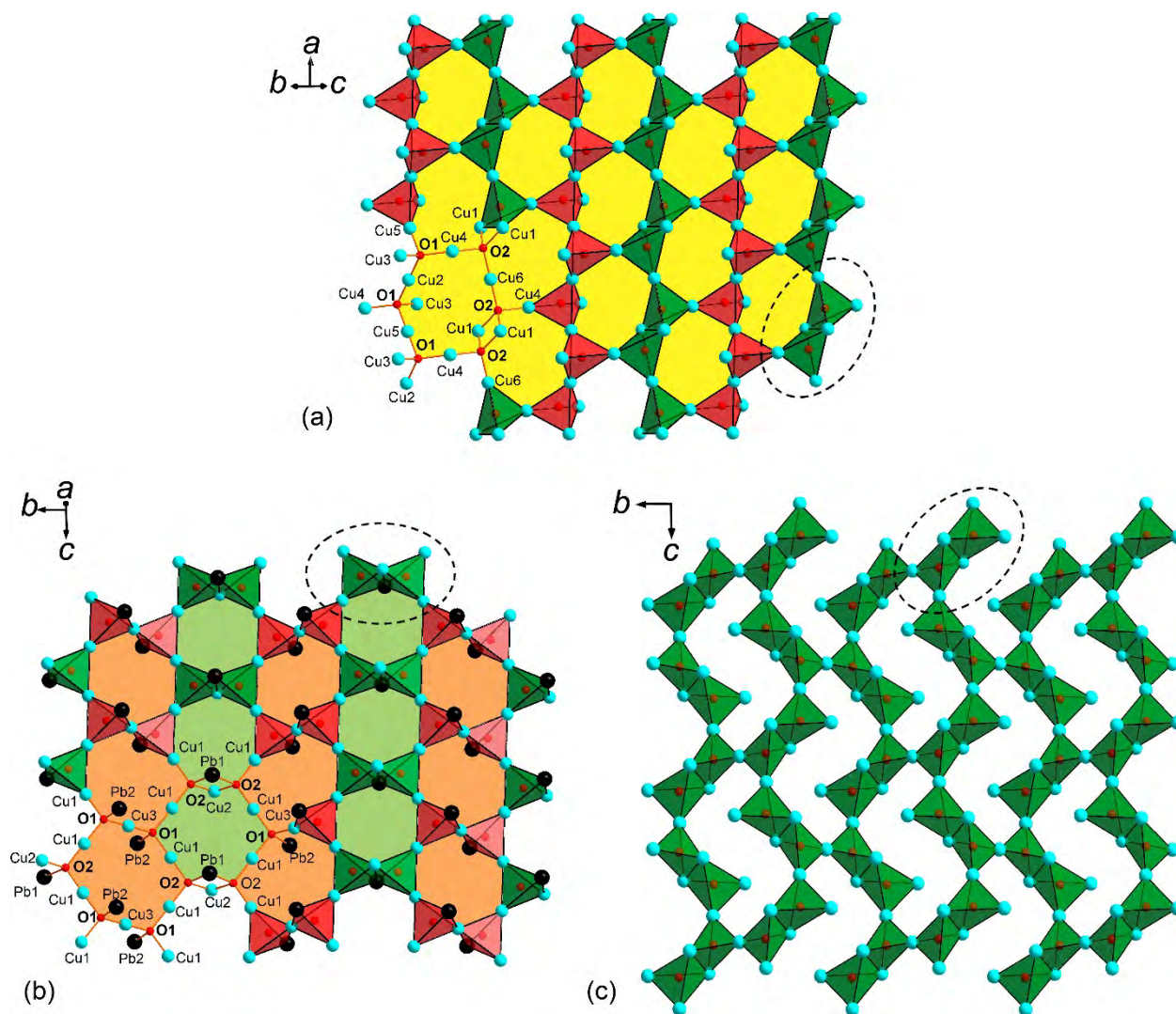


Figure 5. $\overset{2}{\infty}[A_9O_4]^{10+}$ ($A = Cu^{2+}, Pb^{2+}$) layers in minerals and synthetic compounds. General projection of the $\overset{2}{\infty}[Cu_9O_4]^{10+}$ layer in the crystal structure of karlditmarite (a) (O1Cu₄ tetrahedra = red; O2Cu₄ tetrahedra = green; six-membered rings are highlighted in yellow). General projection of the $\overset{2}{\infty}[Cu^{2+}_6Pb_3O_4]^{10+}$ layer in the crystal structure of $[Cu^{2+}_6Pb_3O_4](Cu^+Pb_{1.27}Br_{3.54})(SeO_3)_4Br_2$ (Siidra et al. 2018) (b) (O1PbCu₃ tetrahedra = red; O2PbCu₃ tetrahedra = green; two different six-membered rings are highlighted in colors). General projection of the $\overset{2}{\infty}[Cu_9O_4]^{10+}$ layer in vasilsevergenite (Pekov et al. 2021) (c) (OCu₄ tetrahedra = green). See the text for details.

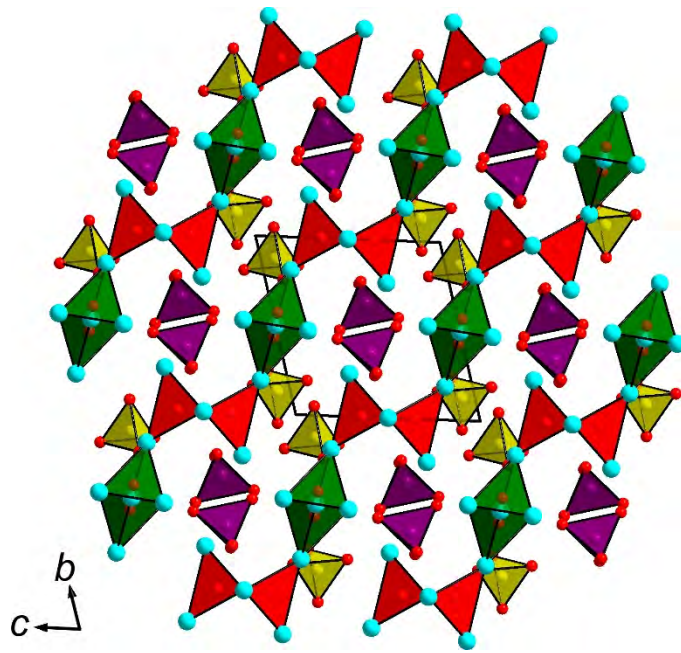


Figure 6. Polyhedral representation of the crystal structure of karlditmarite (O1Cu₄ tetrahedra = red; O2Cu₄ tetrahedra = green; SO₄ tetrahedra = yellow; PO₄ = violet).